Cellular Microbiology (2014) **16**(7), 1080–1093
doi:10.1111/cmi.12262
First published online 13 February 2014

Identification of an endocytic signal essential for the antiviral action of IFITM3

Rui Jia,[1] Fengwen Xu,[2] Jin Qian,[3] Yunfang Yao,[1] Chunhui Miao,[4] Yi-Min Zheng,[4] Shan-Lu Liu,[4] Fei Guo,[2] Yunqi Geng,[1] Wentao Qiao[1] and Chen Liang[3]***

[1]*Key Laboratory of Molecular Microbiology and Biotechnology (Ministry of Education) and Key Laboratory of Microbial Functional Genomics (Tianjin), College of Life Sciences, Nankai University, Tianjin 300071, China.*

[2]*Institute of Pathogen Biology, Chinese Academy of Medical Science & Peking Union Medical College, Beijing 100730, China.*

[3]*Lady Davis Institute, Jewish General Hospital, Montreal, Qc, Canada H3T 1E2.*

[4]*Department of Molecular Microbiology & Immunology, School of Medicine, Bond Life Sciences Center, University of Missouri, Columbia, MO 65211-7310, USA.*

Summary

Members of the interferon-induced transmembrane (IFITM) protein family inhibit the entry of a wide range of viruses. Viruses often exploit the endocytosis pathways to invade host cells and escape from the endocytic vesicles often in response to low pH. Localization to these endocytic vesicles is essential for IFITM3 to interfere with the cytosolic entry of pH-dependent viruses. However, the nature of the sorting signal that targets IFITM3 to these vesicles is poorly defined. In this study, we report that IFITM3 possesses a YxxΦ sorting motif, i.e. 20-YEML-23, that enables IFITM3 to undergo endocytosis through binding to the μ2 subunit of the AP-2 complex. IFITM3 accumulates at the plasma membrane as a result of either mutating 20-YEML-23, depleting the μ2 subunit or over-expressing μ2 mutants. Importantly, blocking endocytosis of IFITM3 abrogates its ability to inhibit pH-dependent viruses. We have therefore identified a critical sorting signal, namely 20-YEML-23, that controls both the endocytic trafficking and the antiviral action of IFITM3. This finding also reveals that as an endocytic protein, IFITM3 first arrives at the plasma membrane before it is endocytosed and further traffics to the late endosomes where it acts to impede virus entry.

Received 25 November, 2013; revised 19 December, 2013; accepted 10 January, 2014. For correspondence. *E-mail chen.liang@mcgill.ca; Tel. (+1) 514 3408260; Fax (+1) 514 3407537; **E-mail wentaoqiao@nankai.edu.cn; Tel. (+86) 22 23503091; Fax (+86) 22 23501783.

Introduction

Many viruses enter cells through endocytosis after binding to receptors on the cell surface (Mercer *et al.*, 2010). In addition to the lipid membranes that pose a physical barrier to virus entry, membrane-associated proteins can deter virus entry by altering the biophysical properties of lipid membranes (Schoggins and Randall, 2013). One example of these proteins is the interferon-induced transmembrane (IFITM) proteins that inhibit the entry of diverse viruses such as influenza A virus (IAV), flaviviruses, filoviruses and others (Diamond and Farzan, 2013; Perreira *et al.*, 2013).

Humans have five IFITM proteins, known as IFITM1, 2, 3, 5 and 10 (Siegrist *et al.*, 2011). IFITM5 is only expressed in osteoblasts and participates in bone mineralization and maturation (Moffatt *et al.*, 2008). The function of IFITM10 remains unknown (Hickford *et al.*, 2012). IFITM1, 2 and 3 all respond to stimulation by type I interferon (Lewin *et al.*, 1991), and inhibit many viruses including IAV, flaviviruses (West Nile virus, dengue virus), filoviruses (Ebola virus, Marburg virus), vesicular stomatitis virus (VSV), SARS coronavirus, reovirus, Rift Valley fever virus, hepatitis C virus (HCV), Jaagsiekte sheep retrovirus (JSRV) and human immunodeficiency virus type 1 (HIV-1) (Brass *et al.*, 2009; Jiang *et al.*, 2010; Weidner *et al.*, 2010; Huang *et al.*, 2011; Lu *et al.*, 2011; Schoggins *et al.*, 2011; Chan *et al.*, 2012; Anafu *et al.*, 2013). The *in vivo* importance of IFITM3 in antiviral defence is demonstrated by the much higher mortality and morbidity of *ifitm3*-knockout mice upon IAV infection as compared to the wild-type mice (Bailey *et al.*, 2012; Everitt *et al.*, 2012). In addition, the hospitalized IAV patients showed significant enrichment of a single-nucleotide polymorphism (SNP) in the *ifitm3* gene that impairs the anti-IAV function of IFITM3 (Everitt *et al.*, 2012; Zhang *et al.*, 2013), although an association of this SNP with mild influenza but not severe H1N1 infection was also reported (Mills *et al.*, 2013). One mechanism of this *in vivo* role of IFITM3 is that its expression protects the lung

resident memory CD8(+) T cells from infection by influenza viruses as well as from subsequent virus exposures (Wakim *et al*., 2013).

IFITM proteins cause accumulation of IAV particles in the intracellular acidic membrane compartments where IFITM proteins predominantly reside (Feeley *et al*., 2011; Huang *et al*., 2011), which suggests a block at virus cytosolic entry. An inhibition of membrane fusion by IFITM was shown by the reduction of cell to cell fusion that is mediated by the envelope proteins of IAV and JSRV as well as other class II and III fusion proteins (Li *et al*., 2013). This inhibition of cell fusion is rescued by a lipid analogue known as oleic acid that confers negative membrane curvature and promotes membrane hemifusion, suggesting that IFITM proteins impede the creation of hemifusion (Li *et al*., 2013). The underlying mechanism may involve decrease in membrane fluidity (Li *et al*., 2013), which is supported by an elevation of cholesterol in multivesicular bodies and late endosomes as a result of IFITM3 interaction with VAPA (Vesicle-membrane-protein-associated protein A) and consequently the dissociation of VAPA from the cholesterol sensor OSBP (oxysterol-binding protein) (Amini-Bavil-Olyaee *et al*., 2013).

IFITM proteins inhibit viruses that enter cells at different subcellular sites. Among these viruses under IFITM inhibition, HIV-1 entry is pH-independent and is generally believed to occur at the plasma membrane (Blumenthal *et al*., 2012). VSV and IAV are pH-dependent viruses, but require different pH optima to trigger viral membrane fusion. VSV entry occurs at pH 6.2 in the early endosome, whereas the membrane fusion of IAV takes place at pH 5.5 in late endosomes and lysosomes (Vazquez-Calvo *et al*., 2012). In order to inhibit these diverse viruses, IFITM proteins need to be present at these various portals of virus entry. Indeed, in addition to endoplasmic reticulum (ER), where they are synthesized and modified, IFITM1, 2 and 3 are also located at the plasma membrane, endosomes and lysosomes, albeit at different levels (Yount *et al*., 2010; 2012; Feeley *et al*., 2011; Huang *et al*., 2011; Li *et al*., 2013). Currently, it is largely unclear what is the trafficking itinerary of IFITM proteins between these cellular membrane compartments, what signals control IFITM trafficking, and how the signalling mechanisms regulate the antiviral action of IFITM proteins. In addition to the roles of palmitoylation and ubiquitination in modulating the subcellular localization of IFITM3 (Yount *et al*., 2010; 2012), a key role of the Y20 residue in this regard has also been reported (Jia *et al*., 2012; John *et al*., 2013). Yet, the mechanism behind this role of Y20 has not been experimentally demonstrated. Here, we provide evidence that IFITM3 bears a tyrosine-based classic sorting signal, 20-YEML-23 of which Y20 is located, that enables IFITM3 to undergo endocytosis and is essential for IFITM3 to inhibit viruses. Although the sorting function of 20-YEML-23 *per se* is not a surprise, our results demonstrate IFITM3 as an endocytic protein and more importantly, this property is essential for IFITM3 to inhibit pH-dependent viruses that enter cells via endocytosis.

Results

The 20-YEML-23 motif allows IFITM3 to undergo endocytosis

The N-terminal region of IFITM3 contains a 20-YEML-23 tetrapeptide that conforms to the canonical YxxΦ sorting signal (x can be any amino acid, Φ denotes amino acid with a bulky side-chain) (Fig. 1A) (Bonifacino and Traub, 2003). In order to determine whether 20-YEML-23 is functionally important for IFITM3 trafficking, we mutated the conserved Y20 and L23 residues and generated a group of IFITM3 mutants (Fig. 1A). We first characterized these mutants by examining their subcellular localizations. We found that, in contrast to the wild-type IFITM3, which is colocalized with endocytosed transferrin, all mutants were accumulated at the cell periphery (Fig. 1B). This observation supports our previous finding that deletion of Y20 causes relocalization of IFITM3 to the plasma membrane (Jia *et al*., 2012). These data together suggest the importance of 20-YEML-23 in determining the subcellular distribution of IFITM3.

Accumulation of the IFITM3 mutants at the plasma membrane suggests that plasma membrane is likely one intermediate site of the wild-type IFITM3 *en route* to late endosomes where wild-type IFITM3 predominantly resides (Feeley *et al*., 2011). To demonstrate this, we first tried to detect cell surface IFITM3 by immunostaining. The N-Flag IFITM3 (with a Flag tag added to the N-terminus) was expressed in HEK293 cells followed incubating the cells with anti-Flag antibody on ice for 30 min. We washed off the unbound antibodies, fixed the cells and imaged for cell surface IFITM3. No apparent fluorescence signal was detected from intact non-permeabilized cells, although the presence of intracellular IFITM3 was shown by the results of staining the detergent-permeabilized cells (Fig. S1). Similarly, the N-Flag YLAA mutant was undetectable on the cell surface with the anti-Flag antibody staining, although this mutant was clearly located at the plasma membrane (Fig. S1). This result suggests that the N-terminal region of IFITM3 is located within the cytoplasm, which is consistent with the published data (Yount *et al*., 2012; Bailey *et al*., 2013).

We next added the Flag tag to the C-terminus of IFITM3 and performed the same experiments. In contrast to the N-Flag IFITM3, the C-Flag version was readily detected on the cell surface with anti-Flag antibody staining at 4°C, suggesting extracellular exposure of the C-terminal

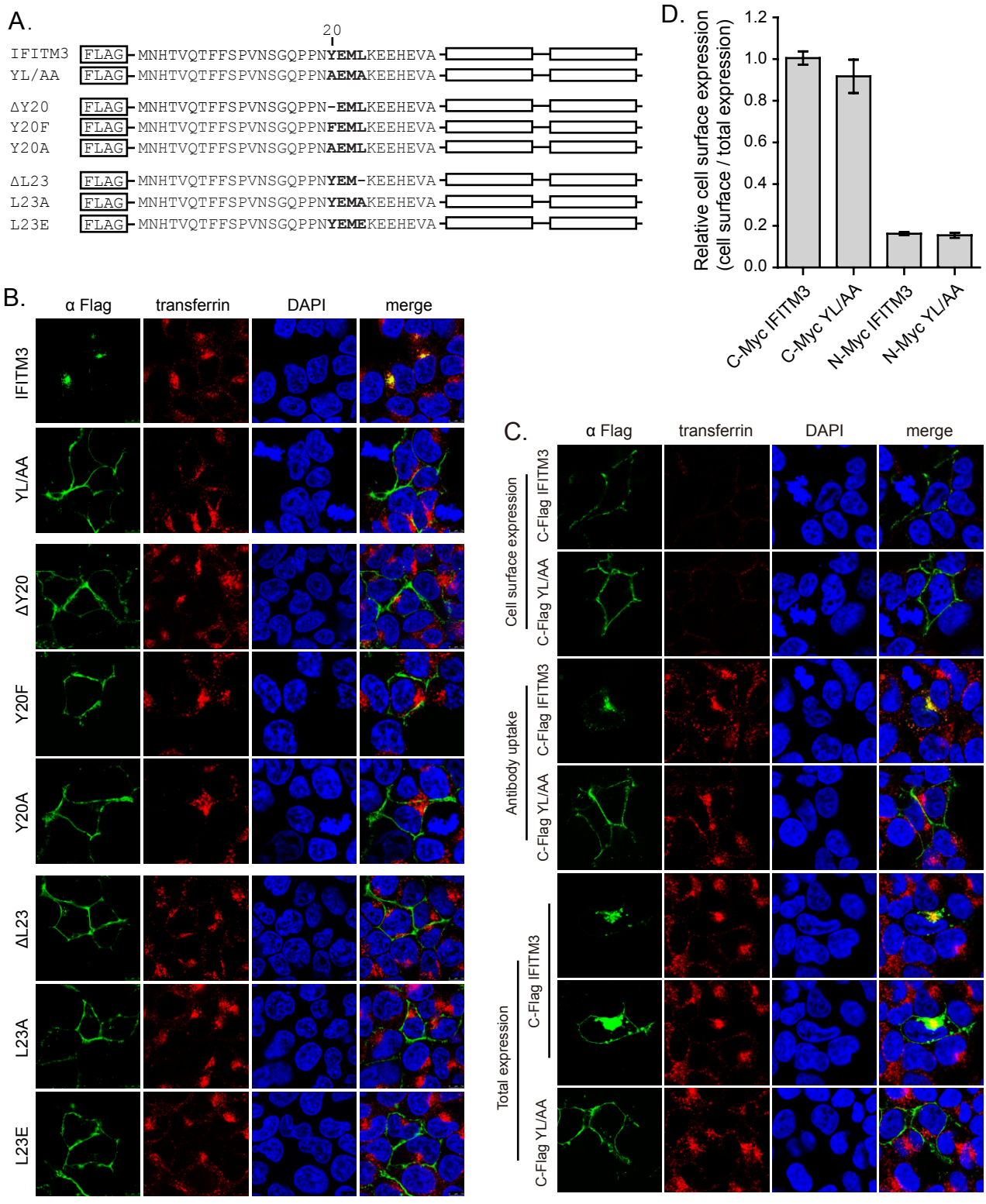
A.
20
IFITM3 FLAG MNHTVQTFFSPVNSGQPPNYEMLKEEHEVA
YL/AA FLAG MNHTVQTFFSPVNSGQPPNAEMAKEEHEVA
ΔY20 FLAG MNHTVQTFFSPVNSGQPPN-EMLKEEHEVA
Y20F FLAG MNHTVQTFFSPVNSGQPPNFEMLKEEHEVA
Y20A FLAG MNHTVQTFFSPVNSGQPPNAEMLKEEHEVA
ΔL23 FLAG MNHTVQTFFSPVNSGQPPNYEM-KEEHEVA
L23A FLAG MNHTVQTFFSPVNSGQPPNYEMAKEEHEVA
L23E FLAG MNHTVQTFFSPVNSGQPPNYEMEKEEHEVA
D.
Relative cell surface expression (cell surface / total expression)
1.2
1.0
0.8
0.6
0.4
0.2
0.0
C-Myc IFITM3
C-Myc YL/AA
N-Myc IFITM3
N-Myc YL/AA
B.
α Flag
transferrin
DAPI
merge
IFITM3
YL/AA
ΔY20
Y20F
Y20A
ΔL23
L23A
L23E
C.
α Flag
transferrin
DAPI
merge
Cell surface expression
C-Flag IFITM3
C-Flag YL/AA
Antibody uptake
C-Flag IFITM3
C-Flag YL/AA
Total expression
C-Flag IFITM3
C-Flag YL/AA

Fig. 1. The YEML motif regulates the subcellular distribution and endocytosis of IFITM3.
A. IFITM3 and its YEML mutations. The 20-YEML-23 motif is highlighted in boldface letters. The unfilled boxes denote the two putative membrane domains.
B. Effect of mutating the YEML motif on cellular localization of IFITM3. HEK293 cells were transfected with IFITM3 or its YEML mutants, then fed with Alexa 555-conjugated transferrin at 37°C for 15 min prior to fixation. IFITM3 proteins were stained with anti-Flag primary antibody and FITC-conjugated secondary antibody. DAPI was used to stain nuclei.
C. IFITM3 undergoes endocytosis. HEK293 cells expressing C-Flag IFITM3 or the YLAA mutant were incubated with anti-Flag antibody at 4°C for 30 min in the presence of Alexa 555-conjugated transferrin. Cells were either fixed directly and stained with anti-Flag antibody (cell surface expression) or switched to 37°C for 15 min to allow internalization of IFITM3/anti-Flag antibody complex (antibody uptake). The internalized complexes were then visualized by staining with FITC-conjugated secondary antibody. To visualize the total IFITM3 or YLAA mutant (total expression), cells were permeabilized with 0.2% saponin prior to immunostaining with anti-Flag antibody. For wild-type IFITM3, two exposures of the same image are presented to show the relatively weak staining at the plasma membrane. Representative images are shown.
D. Cell surface expression of the N- and C-termini of IFITM3. HEK293 cells were transfected with the N- or C-Myc IFITM3 and the YLAA mutant DNA. Half of the cells were incubated with anti-Myc antibody at 4°C to stain the N- or C-terminus of IFITM3 at the cell surface. The other half were fixed and permeabilized with 0.2% saponin, followed by anti-Myc antibody staining for the total expression of IFITM3. Myc-positive cells were scored by flow cytometry. The ratios of Myc-positive cells between the cell surface staining and the total expression staining were calculated to determine the relative cell-surface exposure of the N- and C-termini of IFITM3. The averages of three independent experiments are summarized in the bar graph.

sequence of IFITM3 (Fig. 1C). Not surprisingly, the C-Flag YLAA mutant was also detected on the cell surface with anti-Flag antibody (Fig. 1C). We then performed the antibody uptake experiments by switching the cells to 37°C for 15 min following incubation with anti-Flag antibody on ice. The anti-Flag antibody-bound C-Flag IFITM3 was detected inside the cells and colocalized with the endocytosed transferrin (Fig. 1C). However, the C-Flag YLAA mutant remained at cell periphery, suggesting a defect in endocytosis (Fig. 1C). To validate this observation, we added a different tag, the Myc tag, to the N- or C-terminus of IFITM3 and performed the same antibody uptake and immunostaining experiments. Again, the C-Myc IFITM3, not the N-Myc form, was detected by the anti-Myc antibody at the cell surface, and the C-Myc IFITM3/anti-Myc antibody complex was internalized following incubation at 37°C (Fig. S2A and B). In order to validate the imaging data showing the luminal/extracellular exposure of the C-terminus of IFITM3, we used flow cytometry to score the cells that were stained with the anti-Myc antibody either under the non-permeabilization condition (cell surface expression) or under the permeabilization condition (total expression). Equal numbers of positively stained cells were measured for C-Myc IFITM3 regardless the cells were permeabilized or not, as opposed to the N-Myc IFITM3 whose cell-surface expression was seen in less than 20% of IFITM3-expressing cells (Fig. 1D). Our data support the model that IFITM3 is a type II transmembrane protein (Bailey *et al*., 2013).

In order to further validate that IFITM3 undergoes endocytosis, we treated IFITM3-expressing HEK293 cells with endocytosis inhibitors dynasore or CPZ (Macia *et al*., 2006; Vercauteren *et al*., 2010). A 60 min treatment with dynasore, as compared to the 15 min treatment, more effectively blocked the endocytosis of transferrin and caused relocation of IFITM3 to the plasma membrane (Fig. 2A). Similar effect was observed with CPZ treatment (Fig. 2B). Together, we conclude that IFITM3 is endocytosed from the cell surface and that this process is dependent on the 20-YEML-23 motif.

IFITM3 specifically binds to the μ2 subunit of the AP-2 complex

The YxxΦ sorting signal is recognized by the μ subunit of the AP complex. Five AP complexes have been discovered among which AP-1, 2, 3 and 4, are well characterized (Bonifacino and Traub, 2003; Hirst *et al*., 2011). Each AP has one μ subunit except for AP-1 and AP-3 that have two isoforms of μ. To determine which of these μ subunits recognizes the 20-YEML-23 motif in IFITM3, we expressed the Flag-IFITM3 along with each of μ1A-Myc, μ1B-Myc, μ2-Myc, μ3A-Myc, μ3B-Myc or μ4-Myc. The μ-Myc proteins were immunoprecipitated with anti-Myc antibody, and the presence of IFITM3 in the precipitated materials was examined in Western blotting. The results showed that IFITM3 was co-immunoprecipitated with the μ2 subunit, but not evidently with other μ subunits tested (Fig. 3A). To demonstrate that this interaction is mediated by the 20-YEML-23 motif, IFITM3 mutants with changes in this peptide motif were tested for co-immunoprecipitation with μ2. None of these mutants was associated with the μ2 subunit (Fig. 3B). We noticed that the IFITM3 mutants, except for Y20F, migrated slower than the wild type, which may result from altered protein folding and/or loss of modification at Y20. We further tested two μ2 mutants, WR/AA and FD/AS in which the YxxΦ-binding pocket are mutated (Carvajal-Gonzalez *et al*., 2012). Again, we did not observe any interaction of these two mutants with wild-type IFITM3 (Fig. 3C). Together, these data demonstrate a YEML-dependent interaction between IFITM3 and the μ2 subunit. This specific interaction may result from either the frequent trafficking of IFITM3 from the plasma membrane to the endosomes and/or the high affinity of the YEML motif

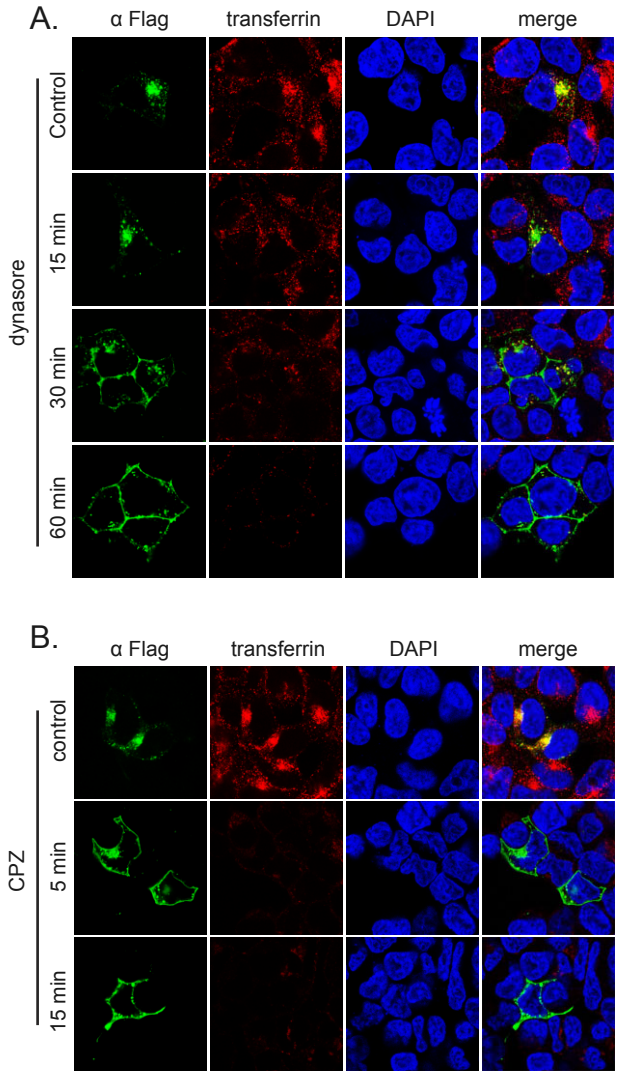

Fig. 2. Dynasore and CPZ block IFITM3 endocytosis. HEK293 cells were transfected with Flag-IFITM3-Flag plasmid DNA. Twenty-four hours after transfection, cells were treated with dynasore (160 μM) (A) or CPZ (20 μg ml^{-1}) (B) for different periods of time, followed by immunostaining Flag-IFITM3. After treatment with dynasore or CPZ, cells were also incubated with Alexa 555-conjugated transferrin (5 μg ml^{-1}) at 37°C for 10 min to monitor the effectiveness of these treatments on endocytosis. Subcellular localization of Flag-IFITM3 was determined by staining with anti-Flag antibody. Nuclei were stained with DAPI. Representative images are shown.

for the μ2 subunit. Our data do not completely exclude the possible weak interactions of IFITM3 with other μ subunits. In support of this possibility, it has been shown that, in spite of the high affinity of the YEVM motif of the lysosomal protein CD63 for the μ3 subunit, mutating μ3 mislocalizes CD63 to the plasma membrane, which reveals the interaction of YEVM with μ2 in the absence of wild-type μ3 (Rous *et al*., 2002).

Depleting endogenous μ2 disrupts the subcellular localization of IFITM3

We next asked if the μ2 subunit is functionally involved in the endocytosis of IFITM3. We first examined the effect of the two μ2 mutants WR/AA and FD/AS on the subcellular distribution of IFITM3. In contrast to the ectopic expression of the wild-type μ2 subunit that did not affect the intracellular localization of IFITM3, the WR/AA and FD/AS mutants caused accumulation of IFITM3 on cell periphery, likely as a result of disrupting the function of endogenous AP-2 complex (Fig. 4A). We next knocked down μ2 with siRNA oligos (Fig. 4B) and examined how cellular distribution of IFITM3 was affected. The results showed that μ2 knock-down effectively blocked the endocytosis of transferrin (Fig. 4C). The same μ2 siRNA treatment led to the accumulation of IFITM3 at cell periphery (Fig. 4C). Although none of the four siRNA oligos completely depleted endogenous μ2 (Fig. 4B), internalization of transferrin and IFITM3 was drastically reduced, which suggests that the level of μ2 is a key determinant of endocytosis efficiency. We extended this study to knock down μ2 in HeLa cells, and observed that, concomitant with the blockade of transferrin endocytosis, the endogenous IFITM3 was re-located from intracellular compartments to the plasma membrane (Fig. 4D). Taken together, we conclude that the μ2 subunit of AP-2 complex is functionally required for the endocytosis of IFITM3.

Mutating the 20-YEML-23 motif limits the antiviral function of IFITM3

We next examined whether the antiviral action of IFITM3 depends on the integrity of the 20-YEML-23 motif. In this context, we generated HEK293 cell lines that stably expressed either the wild-type IFITM3 or the mutants with altered 20-YEML-23 sequence. We then challenged these HEK293 cells with IAV [A/WSN/33 (H1N1)], and assessed virus infection by measuring the levels of IAV proteins NP, M2 and HA by Western blotting. A drastic decrease in the levels of NP, M2 or HA was observed in IFITM3-expressing cells as compared to the control cells (Fig. 5A). In contrast, similar levels of IAV infection were observed in both control cells and cells expressing IFITM3 mutants (Fig. 5A). The loss of IAV inhibition by these IFITM3 mutants is not due to their poor expression because they were expressed as well as the wild-type IFITM3 (Fig. 5A). We further assessed the anti-IAV activities of wild-type IFITM3 and its mutants using various doses of IAV for infection and scored the viral NP-positive cells by flow cytometry. With the lowest dose of IAV that infected 13% of cells, IFITM3 reduced the number of infected cells by 17-fold, whereas the Y20A, L23A and YLAA mutants exhibited a threefold inhibition (Fig. 5B and Fig. S3). At the highest dose of viruses that infected over

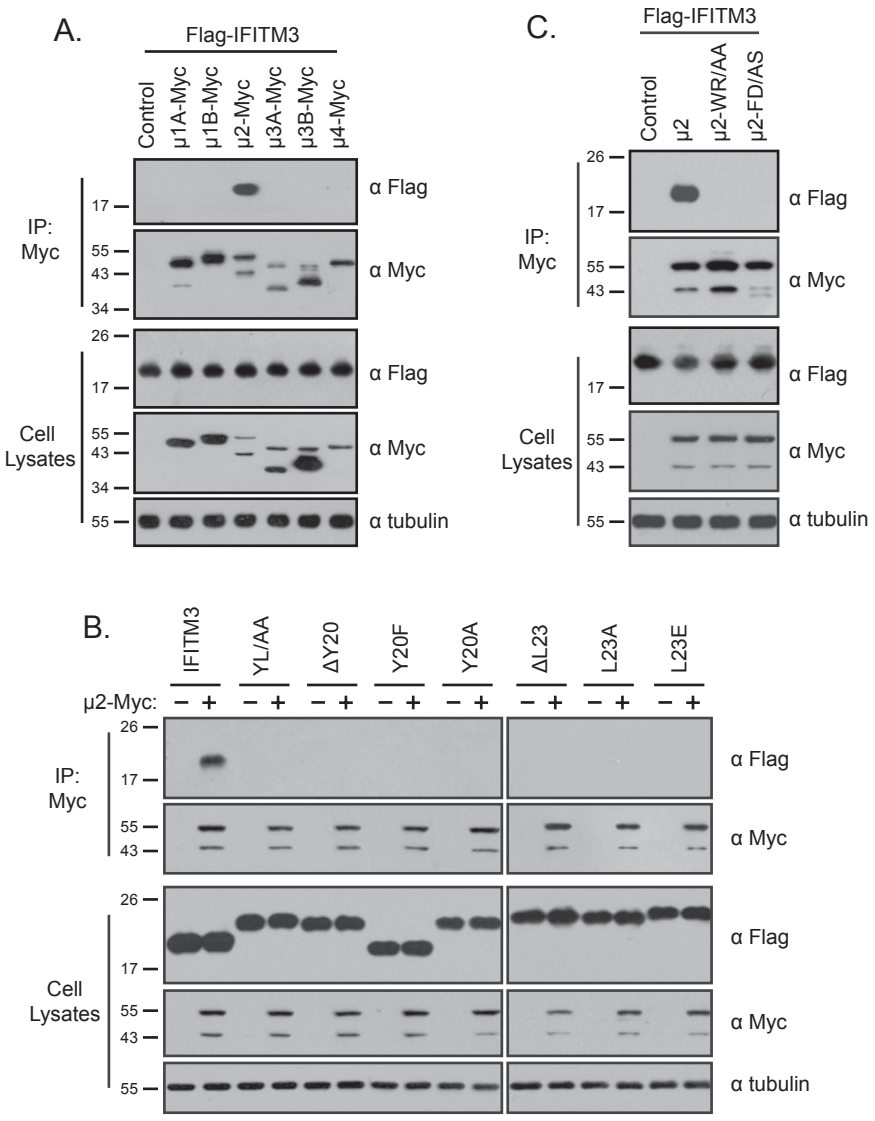

Fig. 3. IFITM3 interacts with the μ2 subunit of AP-2 complex.
A. Co-immunoprecipitation of IFITM3 with the μ subunits. HEK293T cells were transfected with plasmid DNA expressing Flag-IFITM3 and Myc-tagged μ subunits. Myc-μ proteins were immunoprecipitated with anti-Myc antibody, followed by Western blotting with the indicated antibodies.
B. Co-immunoprecipitation to examine the association of μ2 with IFITM3 mutants that had the YEML sequence altered.
C. Co-immunoprecipitation to detect the interaction of IFITM3 with μ2 mutants WR/AA and FD/AS that bear mutated YxxΦ-binding pocket.
Sizes of protein markers (in kDa) are shown on the left side of each Western blot.

90% of cells, IFITM3 still strongly inhibited IAV infection, as opposed to the Y20A, L23A and YLAA mutants that completely lost their inhibitory effects (Fig. 5B and Fig. S3).

We further tested how mutating the 20-YEML-23 motif affects IFITM3 to inhibit viral infections that were mediated by the VSV G protein (pH-dependent entry), Ebola virus GP protein (pH-dependent entry), as well as the MLV 10A1 protein (pH-independent entry). Again, mutating YEML disabled IFITM3 from inhibiting VSV G and Ebola GP-mediated infection (Fig. 5C). Noticeably, while IFITM3 did not inhibit 10A1-meidated infection, the YL/AA mutant exerted moderate inhibitory effect (Fig. 5C). Together, these data demonstrate that the 20-YEML-23 motif is important for IFITM3 to inhibit pH-dependent virus entry.

YEML is functionally conserved in IFITM3 of different species

IFITM3 is known to be conserved in many species (Hickford *et al.*, 2012). Alignment of their sequences revealed the presence of a YEML-like motif at similar locations at their N-terminal regions (Fig. 6A). Among

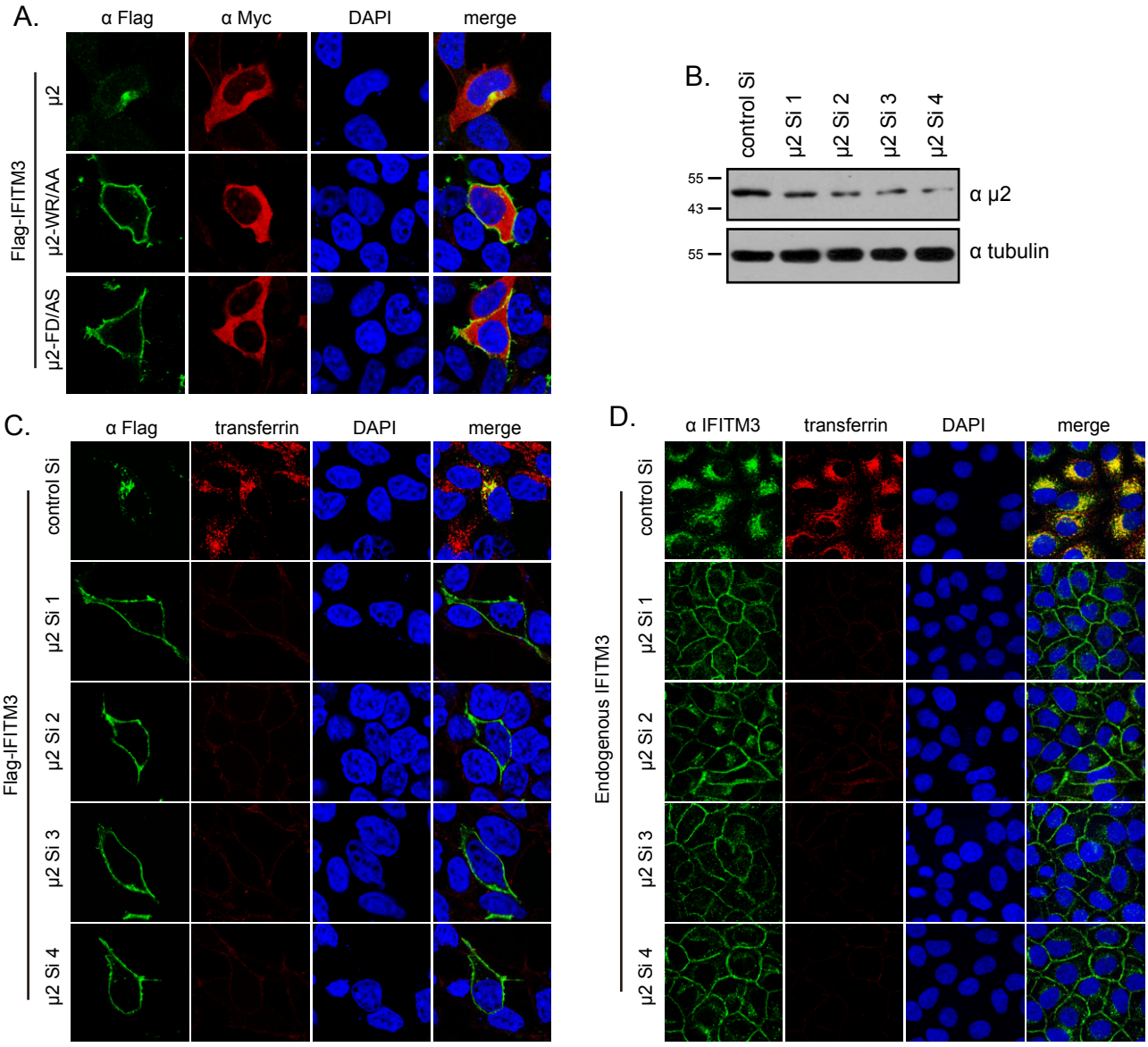

Fig. 4. Effect of modulating μ2 level on subcellular distribution of IFITM3.
A. The μ2 mutants WR/AA and FD/AS were ectopically expressed in HEK293 cells together with Flag-IFITM3. Cellular localizations of Flag-IFITM3 (pseudocoloured as green) and μ2 mutants (pseudocoloured as red) were determined by staining with anti-Flag and anti-Myc antibodies respectively. DAPI was used to stain nuclei. Representative images are shown.
B. HEK293 cells were transfected with siRNA oligonucleotides targeting μ2. Levels of endogenous μ2 were measured by Western blotting with anti-μ2 antibody. Tubulin was probed as an internal control. Sizes of protein markers (in kDa) are shown.
C. Depletion of μ2 causes accumulation of Flag-IFITM3 at the plasma membrane. HEK293 cells were transfected with siRNA targeting μ2 and IFITM3 plasmid DNA. Localization of IFITM3 was determined by staining with anti-Flag antibody. Transferrin internalization was used to monitor the effect of μ2 knock-down on endocytosis.
D. Effect of μ2 knock-down on subcellular distribution of endogenous IFITM3 in HeLa cells. The endogenous IFITM3 was detected with anti-IFITM3 antibody. The endocytosis efficiency was monitored by measuring the internalization of transferrin. Representative images are shown.

these four amino acids, Met appears to be the least conserved. In order to test whether this sequence divergence affects the antiviral activity of IFITM3, we exchanged the YxxΦ motif between human IFITM3 (YEML) and mouse IFITM3 (YERI), and determined how this change affects their ability to inhibit IAV infection. Both the wild-type and mutated IFITM3 proteins were expressed at similar levels except that the YEML motif diminished protein migration on the SDS-PAGE (Fig. 6B). Nevertheless, such an exchange in YxxΦ motif did not affect the anti-IAV abilities of either human IFITM3 or mouse IFITM3 (Fig. 6C and D), suggesting that they are functionally inter-changeable.

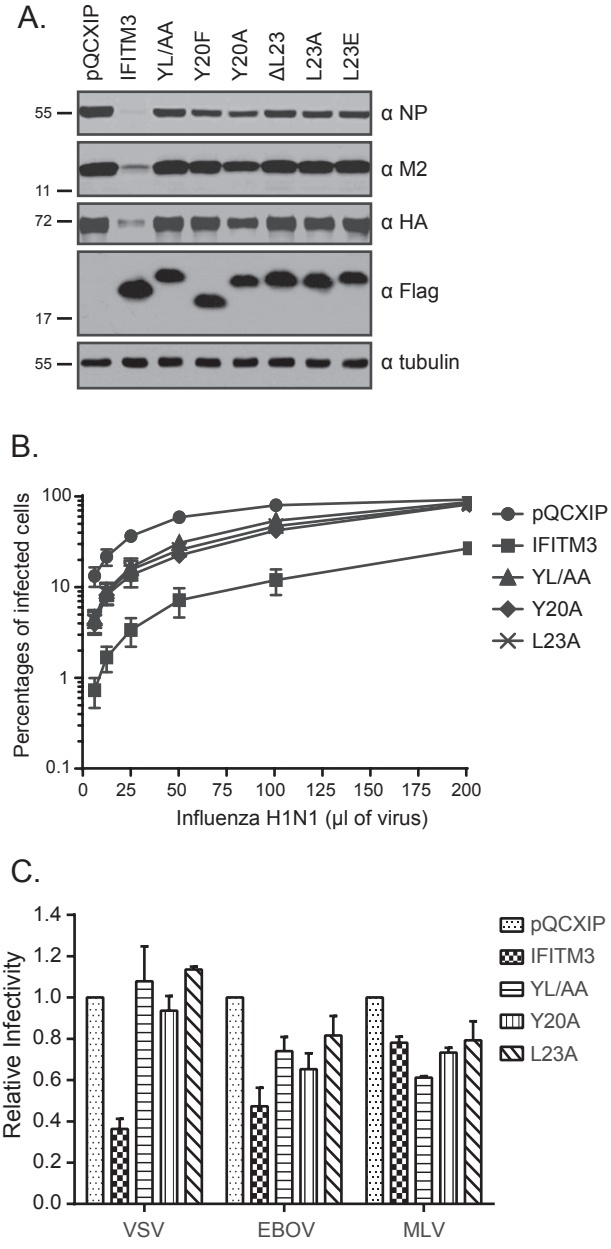

Fig. 5. Mutating the YEML motif diminishes the capacity of IFITM3 to inhibit viruses.
A. IAV was used to infect HEK293 cells that stably express IFITM3 or its mutants with altered YEML sequence. Eight hours after infection, cells were lysed and the levels of IAV proteins NP, M2 and HA were determined by Western blotting. Anti-Flag antibody was used to probe the ectopically expressed IFITM3 and its mutants. Sizes of protein markers are shown on the left side of the Western blots.
B. Different doses of IAV were used to infect the IFITM3-expressing HEK293 cell lines. Eight hours after infection, the infected cells were fixed and stained with anti-NP antibody followed by flow cytometry analysis to score the infected cells. Results shown are the average of three independent infections. The original flow cytometry data are presented in supplemental Fig. S3.
C. Effects of wild-type IFITM3 and its mutants on infections that were mediated by VSV G protein, Ebola virus GP and the 10A1 protein of MLV. The IFITM3-expressing HEK293 cells were infected with the MLV-GFP reporter viruses that were pseudotyped with VSV-G, EBOV GP or 10A1 proteins. GFP-positive cells were scored by flow cytometry 40 h after infection. Results shown are the average of three independent experiments. The *P*-values were calculated between the data of wild-type IFITM3 and those of IFITM3 mutants, the numbers are below 0.05 for infections mediated by VSV G and EBOV GP.

Discussion

Results of this study suggest that the 20-YEML-23 motif of IFITM3 acts as a functional protein-sorting signal through interacting with the μ2 subunit of the AP-2 complex and allows IFITM3 to undergo endocytosis (Fig. 7). Given that many viruses exploit endocytosis to enter cells (Mercer *et al*., 2010), trafficking along the endocytosis pathway provides IFITM3 with the opportunity to encounter and inhibit these viruses (Fig. 7). Regardless whether the virus hijacks the clathrin-dependent or clathrin-independent endocytosis route (Mercer *et al*., 2010), the endocytosed vesicles ultimately fuse with endosomal compartments and deliver their cargos, including the internalized viral particles, to late endosomes and lysosomes where the majority of IFITM3 molecules are located (Feeley *et al*., 2011). This subcellular localization allows IFITM3 to interfere with the entry of diverse viruses that enter cells via different endocytosis pathways. Because different viruses penetrate cellular membranes at different intracellular sites, some in the early endosomes such as VSV, while others in the late endosomes/lysosome such as IAV and EBOV (Fig. 7) (Vazquez-Calvo *et al*., 2012), the extent of susceptibility to IFITM3 restriction likely vary among different viruses. One interesting example is the resistance of arenaviruses to IFITM3 restriction, which likely results from their entry via a clathrin- and caveolin-independent endocytosis pathway (Brass *et al*., 2009).

Subcellular localization and trafficking of IFITM3 can be influenced by post-translational modifications. Three types of post-translational modifications have been reported for IFITM3. The first is S-palmitoylation at cysteines 71, 72 and 105 (Yount *et al*., 2010). Mutating these cysteines do not affect the localization of IFITM3 at ER, but diminishes membrane-binding and clustering properties of IFITM3. As a result, IFITM3 antiviral action is abrogated (Yount *et al*., 2012; John *et al*., 2013). The second is ubiquitination at lysines 24, 83, 88 and 104 with K24 as the major acceptor for ubiquitin (Yount *et al*., 2012). As opposed to S-palmitoylation, eliminating IFITM3 ubiquitination by mutating these lysine residues promotes localization of IFITM3 to late endosomes and concomitantly enhances IFITM3's antiviral activity (Yount *et al*., 2012). One possible explanation is that ubiquitination at K24 occludes the

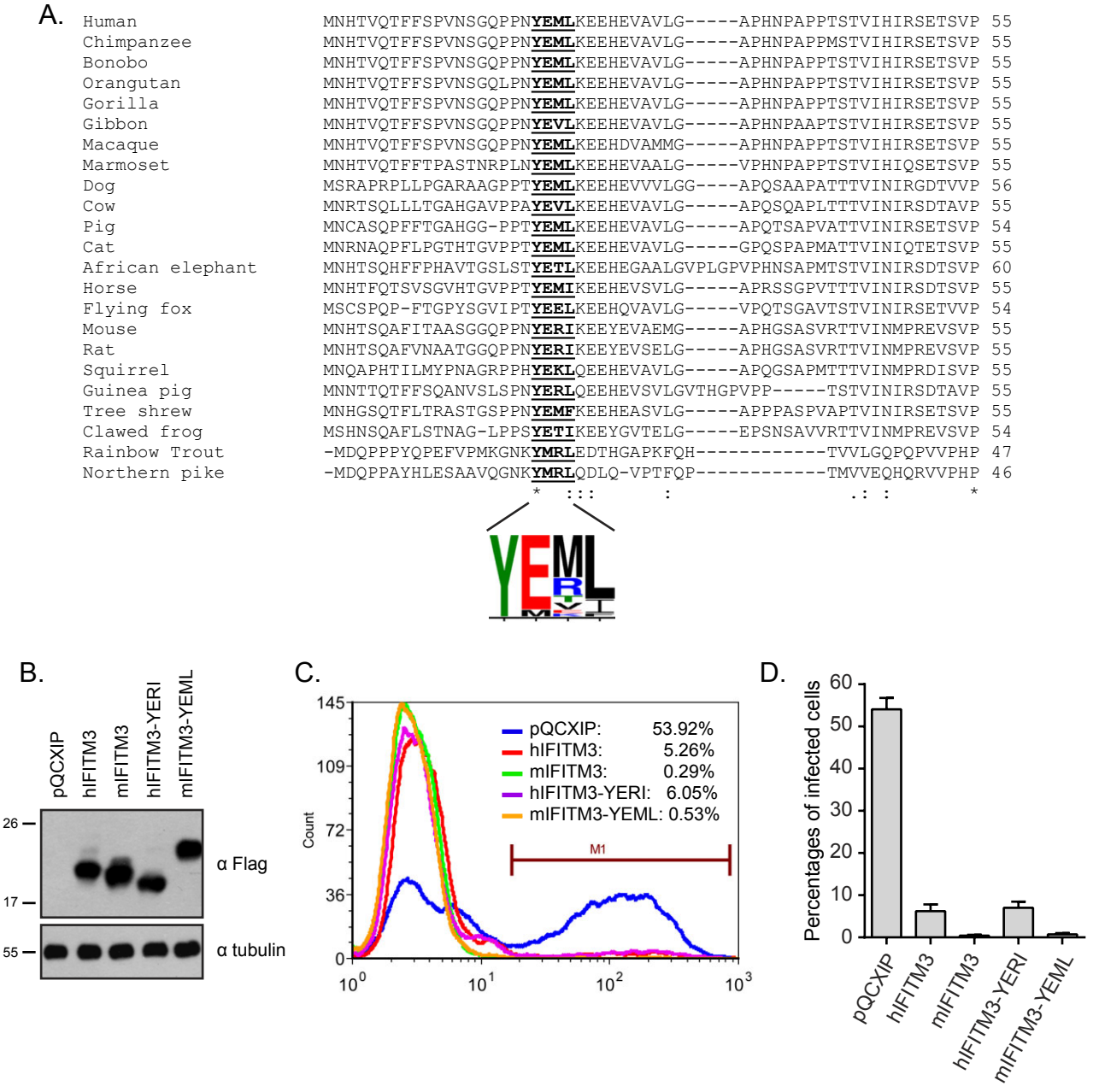

Fig. 6. Effects of different Y-motifs on the antiviral activity of IFITM3.
A. Conservation of the YEML-like motif in IFITM3 proteins from different species. The consensus sequence of this Y-motif is shown.
B. hIFITM3-YERI contains the YERI motif from mouse IFITM3 (mIFITM3), mIFITM3-YEML has the YEML motif from human IFITM3 (hIFITM3). HEK293 cell lines were generated to stably express these IFITM3 proteins. pQCXIP is the empty retroviral vector and was used to produce the control cell line. Expression levels of IFITM3 proteins were determined by Western blotting. Sizes of protein markers are shown on the left side of the Western blots.
C. The IFITM3-expressing HEK293 cell lines were infected with IAV. Cells were collected 8 h after infection, then immunostained for viral NP protein. The positive cells were scored by flow cytometry.
D. Results of three independent infections are summarized in the bar graph.

recognition of the proximal 20-YEML-23 sorting motif by μ2 subunit of the AP-2 complex and thus impairs IFITM3 endocytosis (Fig. 7). Lastly, the Y20 amino acid is phosphorylated by the Fyn tyrosine kinase (Jia *et al.*, 2012). Given that tyrosine phosphorylation in the YxxΦ motif hinders the recognition by μ2 and consequently impedes AP-2-dependent endocytosis (Bonifacino and Traub, 2003), it is likely that Y20 phosphorylation serves as a mechanism for cells to regulate the endocytosis efficiency and the subcellular localization of IFITM3.

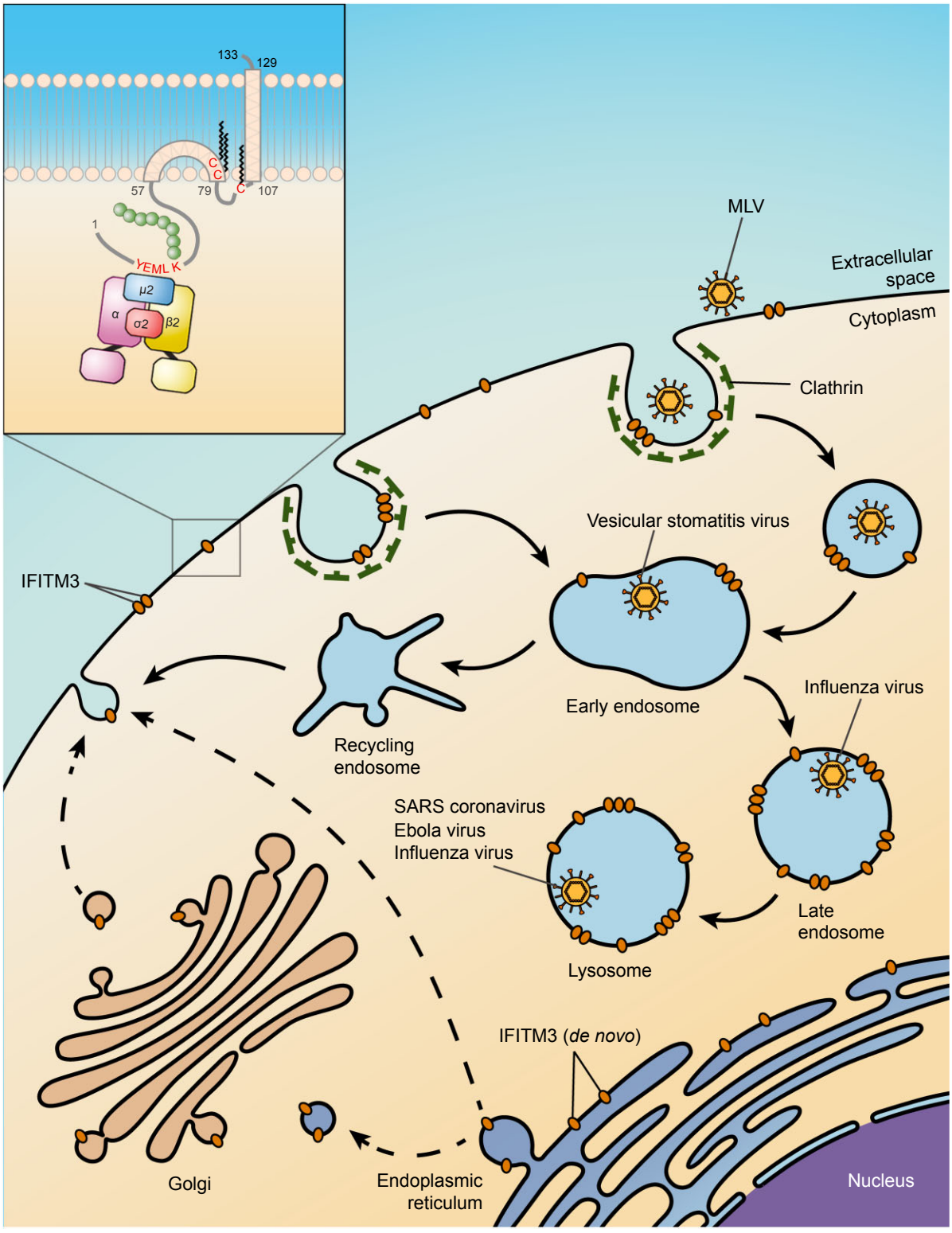

Fig. 7. A model to illustrate the intracellular trafficking of IFITM3 and its antiviral action. Following its synthesis at the ER, IFITM3 traffics to the plasma membrane where its 20-YEML-23 motif interacts with the μ2 subunit of AP-2 complex and undergoes clathrin-dependent endocytosis. Ubiquitination of K24 is shown. C71/72/105 are palmitoylated. This trafficking mechanism positions IFITM3 on the endocytic pathway that many viruses utilize for cell entry. Examples of these viruses are VSV, IAV and EBOV. MLV is a pH-independent virus. VSV, vesicular stomatitis virus; IAV, influenza A virus; EBOV, Ebola virus; MLV, murine leukaemia virus. This model is partially adapted from those published in Bailey *et al.* (2013), Diamond and Farzan (2013) and Perreira *et al.* (2013).

The critical role of Y20 in the antiviral activity of IFITM3 has been reported in other studies. Deleting the first 21 amino acids prevents IFITM3 from inhibiting VSV and IAV (Weidner *et al*., 2010; Everitt *et al*., 2012). This loss of virus inhibition can be recapitulated by mutating only Y20 (Jia *et al*., 2012; John *et al*., 2013). In addition, a SNP rs12252-C of IFITM3 is significantly enriched in hospitalized patients who suffered from seasonal and pandemic influenza H1N1/09 viruses (Everitt *et al*., 2012; Zhang *et al*., 2013). This SNP causes aberrant splicing of IFITM3 mRNA and creates an IFITM3 mutant lacking the first 21 amino acids. Discovering 20-YEML-23 as a functional sorting signal provides the molecular mechanism behind the key role of Y20 in IFITM3 antiviral activity that was reported in the above studies. It is noted that IFITM1 does not bear the YEML motif, yet it still exerts antiviral activity. We postulate that its C-terminal sequence, which bears a YHIM motif, may control IFITM1 trafficking and antiviral function.

Results of our study support the type II transmembrane topology of IFITM3 that was recently reported by Bailey *et al*. (2013). Two other membrane topologies of IFITM3 were previously documented. One model stipulates that IFITM3 is a dual-pass transmembrane protein with luminal/extracellular existence of both N- and C-termini. This model is supported by the results of cell surface immunostaining and flow cytometry experiments showing the detection of the Flag tag attached to the N-terminus of IFITM3 (Weidner *et al*., 2010). The second model describes IFITM3 as an intramembrane protein with both termini projecting towards the cytoplasm. In support of this latter membrane topology, none of the putative glycosylation sites within the distal N- or C-terminal region of IFITM3 is modified (Yount *et al*., 2012). Furthermore, the K24 residue in the N-terminal region is ubiquitinated, which can only occur when K24 is exposed to the intracellular E3 ligases. Our results support the cytoplasmic residence of the N-terminal region of IFITM3, since cell surface staining with anti-Flag or anti-Myc antibody barely detected these N-terminal tags. In the meantime, we were able to readily detect, at the cell surface, the Flag or the Myc tag that was added to the C-terminus of IFITM3, which supports the luminal/extracellular exposure of the C-terminal region of IFITM3 (Fig. 7). In further support of the luminal residence of the C-terminus of IFITM3, appending an ER retention signal, KDEL, leads to ER sequestration of IFITM3 (Bailey *et al*., 2013). Moreover, the C-terminus, but not the N-terminus, of IFITM3 is subject to lysosomal degradation (Bailey *et al*., 2013). While more studies are warranted to reconcile these different observations, it is possible that the topologies of IFITM3 on membranes may be dynamic in nature, which depend on the different post-translational modifications in different cell types.

Experimental procedures

Plasmids

The IFITM3, ΔY20, Y20F and Y20A plasmids were described previously (Jia *et al*., 2012). The other IFITM3 mutants YLAA, ΔL23, L23A, L23E, hIFITM3(YERI), mIFITM3(YEML), hIFITM3(YEQF), hIFITM3(YQRL), hIFITM3(YEVM), hIFITM3(YTRF) were generated with a PCR-based mutagenesis method. This PCR-based method was also used to add the Flag tag to the C-terminus of IFITM3, the Myc tag to the N- or C-terminus of IFITM3. The PCR primers are listed in Table S1. The Rab5-GFP expression vector was a gift from Stephen Ferguson (Seachrist *et al*., 2002). The μ1A, μ1B, μ2, μ3A, μ3B and μ4 plasmids were kindly provided by Juan Bonifacino and Heike Fölsch (Folsch *et al*., 2001; Carvajal-Gonzalez *et al*., 2012). A Myc tag was added to the C-terminus of each μ subunit for detection by Western blotting and immunofluorescence staining. Two μ2 mutants, WR/AA and FD/AS, were generated with PCR-based mutagenesis using primers listed in Table S1. Transfection of plasmid DNA into cells was performed with Lipofectamine 2000 (Invitrogen) in accordance with the manufacturer's instruction.

Antibodies and reagents

Anti-AP2M1 (μ2) antibody (cat. number NBP2-00834) was purchased from Novus Biologicals, anti-IFITM3 antibody (cat. number 11714-1-AP) from ProteinTech, anti-NP antibody (Influenza A nucleoprotein) (cat. number MAB8251) from Millipore, anti-Flag M2 antibody (cat. number F1084) from Sigma, and anti-Myc (cat. number sc-789), anti-IAV M2 (cat. number sc-32238), and anti-HA antibodies (cat. number sc-805) from Santa Cruz. FITC- and TRITC-conjugated secondary antibodies (cat. numbers 111-195-003 and 115-095-003) were purchased from Jackson ImmunoResearch Laboratories. Chlorpromazine (CPZ) (cat. number C8138), saponin (cat. number S4521) and dynasore (cat. number D7693) were purchased from Sigma.

Generation of stably transduced cell lines

First, retrovirus particles were prepared by transfecting HEK293T cells with 2 μg pQCXIP-IFITM3 DNA, 2 μg pCMV-MLV-gag-pol DNA and 0.5 μg pVSV-G DNA. After 48 h, supernatants were collected and centrifuged at 3000 r.p.m. to remove cell debris. HEK293 cells were infected with the harvested virus particles in the present of 5 μg ml^{-1} polybrene by spinoculation at 1800 r.p.m. for 45 min at room temperature. Twenty-four hours after infection, cells were selected in complete DMEM medium containing 2 μg ml^{-1} puromycin (Sigma).

Virus infections

IAV infection was conducted as follows. HEK293 cells expressing IFITM3 or its YEML mutants were first washed with 1× phosphate-buffered saline, then exposed to various doses of IAV [strain A/WSN/33 (H1N1)] that were diluted in influenza virus growth medium (Opti-MEM containing 0.5% FBS). One hour after infection, viral inoculums were washed off with growth medium. Cells were maintained in growth medium for 8 more hours before being detached with 5 mM EDTA. The infected cells were lysed

and subjected to Western blotting with anti-Flag, M2, HA or NP antibodies. Alternatively, cells were fixed in 4% formaldehyde (in 1× phosphate-buffered saline), permeabilized with 0.1% Triton X-100 for 10 min, and immunostained with anti-NP antibody. The infected cells were scored by flow cytometry. Infection with MLV-GFP reporter viruses was performed as we previously described (Jia *et al*., 2012). Briefly, the reporter viruses were produced by transfecting HEK293T cells with plasmid DNA pCMV-gag-pol-MLV, pCMV-GFP-MLV, and pVSV-G, pEBOV-GP or p10A1. The viruses were used to infect HEK293 cell lines that express IFITM3 and its mutants. The infected cells were scored for GFP-positive cells by flow cytometry.

Immunoprecipitation and Western blotting

Cells (1×10^7) were lysed in the lysis buffer containing 20 mM Tris (pH 7.4), 150 mM NaCl, 5 mM EDTA, 1% Triton X-100 and protease inhibitors cocktail (Roche). Cell debris was removed by centrifugation, and the cell lysates were incubated with anti-Myc or anti-μ2 antibody for 2 h on ice before protein A resin (Millipore) was added for an overnight incubation. After three times washing with the lysis buffer, the bound proteins were extracted with the 1× loading buffer (containing 1% SDS) at 95°C for 15 min. The protein samples were examined in Western blotting with the following antibodies: anti-Flag (1:10 000), anti-Myc (1:2000), anti-NP (1:5000), anti-HA (1:5000), anti-M2 (1:5000) and anti-μ2 (1:1000).

Immunofluorescence microscopy

HEK293 cells were seeded on poly-lysine-coated glass slides 1 day before transfection with plasmid DNA expressing IFITM3 or its mutants. Forty hours after transfection, cells were incubated with Alexa 555-conjugated transferrin (Invitrogen) (5 μg ml^{-1} in serum-free DMEM) for 15 min at 37°C. After washing with 1× phosphate-buffered saline, cells were first fixed with 4% formaldehyde for 10 min at room temperature, then permeabilized with 0.1% Triton X-100 for 10 min. After incubation in the blocking buffer containing 3% BSA and 6% skim milk, cells were stained with anti-Flag or anti-Myc primary antibodies (1:100 dilution, 2 h at room temperature) followed by FITC- or TRITC-conjugated secondary antibodies (1:100 dilution, 45 min at room temperature). DAPI was utilized to stain nuclei. Images were captured using Leica TCS SP5 laser scanning confocal microscope.

Treatment with dynasore and chlorpromazine (CPZ)

The HEK293 cells were first transfected with Flag-IFITM3 plasmid DNA for 24 h before being treated either with dynasore (160 μM) for 15, 30 and 60 min, or with CPZ (20 μg ml^{-1}) for 5 and 15 min. The cells were then fixed and immunostained for Flag-IFITM3 as described above. To monitor the effect of dynasore or CPZ treatment on endocytosis, cells were incubated with Alexa 555-conjugated transferrin (5 μg ml^{-1}) at 37°C for 10 min. Cells were then washed with 1× phosphate-buffered saline, fixed in 4% formaldehyde and examined under confocal microscope.

Antibody uptake assay

HEK293 cells were transfected with plasmid DNA expressing Flag-tagged IFITM3 or its YLAA mutant. The Flag tag was attached either to the N- or to the C-terminus of IFITM3. Forty hours after transfection, the cells were washed once with 1× phosphate-buffered saline, then incubated with anti-Flag antibody (1 μg μl^{-1}) and Alexa 555-conjugated transferrin (5 μg ml^{-1}, in serum-free DMEM) at 4°C for 30 min. After washing with serum-free DMEM, the cells were incubated at 37°C for 15 min before being fixed with 4% formaldehyde. The internalized IFITM3/anti-Flag complexes were detected by permeabilizing cells with 0.1% Triton X-100 and staining with FITC-conjugated secondary antibody. Images were recorded using Leica TCS SP5 laser scanning confocal microscope.

siRNA knock-down of μ2 subunit

Four μ2 siRNA oligonucleotides were purchased from Qiagen, their sequences are:

siμ2-1 (catalogue number SI00059318): ACGTGTGACTTC GTCCAGTTA;
siμ2-2 (catalogue number SI02632469): TGGAGGCTTATTC ATCTATAA;
siμ2-3 (catalogue number SI02632476): TTGGAGGCTTATT CATCTATA;
siμ2-4 (catalogue number SI02777355): TGCCATCGTGTGGA AGATCAA.

HeLa cells (0.5×10^5) were seeded on the glass slides in the 12-well plate 1 day before transfection with siRNA (20 pmol each well) using Lipofectamine 2000 (Invitrogen). After two sequential siRNA transfections, cells were fed with 5 μg ml^{-1} Alexa 555-conjugated transferrin at 37°C for 15 min and then fixed for immunofluorescence staining with anti-IFITM3 antibody as described above. Levels of endogenous μ2 were determined by Western blotting with anti-μ2 antibody.

Acknowledgements

This study was supported by funds from the Canadian Institutes for Health Research (HVI98828 and MOP-77649), US National Institutes of Health (R21AI105584), the Chinese Ministry of Health (2012ZX 10001-006), the National Natural Science Foundation of China (81271812 and 81071343), New Century Excellent Talents in University (NCET-10-0508) and CSC (China Scholarship Council) State Scholarship Fund.

References

Amini-Bavil-Olyaee, S., Choi, Y.J., Lee, J.H., Shi, M., Huang, I.C., Farzan, M., and Jung, J.U. (2013) The antiviral effector IFITM3 disrupts intracellular cholesterol homeostasis to block viral entry. *Cell Host Microbe* **13:** 452–464.

Anafu, A.A., Bowen, C.H., Chin, C.R., Brass, A.L., and Holm, G.H. (2013) Interferon inducible transmembrane protein 3 (IFITM3) restricts reovirus cell entry. *J Biol Chem* **288:** 17261–17271.

Bailey, C.C., Huang, I.C., Kam, C., and Farzan, M. (2012) Ifitm3 limits the severity of acute influenza in mice. *PLoS Pathog* **8:** e1002909.

Bailey, C.C., Kondur, H.R., Huang, I.C., and Farzan, M. (2013) Interferon-induced transmembrane protein 3 is a type II transmembrane protein. *J Biol Chem* **288:** 32184–32193. doi:10.1074/jbc.M113.514356

Blumenthal, R., Durell, S., and Viard, M. (2012) HIV entry and envelope glycoprotein-mediated fusion. *J Biol Chem* **287:** 40841–40849.

Bonifacino, J.S., and Traub, L.M. (2003) Signals for sorting of transmembrane proteins to endosomes and lysosomes. *Annu Rev Biochem* **72:** 395–447.

Brass, A.L., Huang, I.C., Benita, Y., John, S.P., Krishnan, M.N., Feeley, E.M., *et al*. (2009) The IFITM proteins mediate cellular resistance to influenza A H1N1 virus, West Nile virus, and dengue virus. *Cell* **139:** 1243–1254.

Carvajal-Gonzalez, J.M., Gravotta, D., Mattera, R., Diaz, F., Perez Bay, A., Roman, A.C., *et al*. (2012) Basolateral sorting of the coxsackie and adenovirus receptor through interaction of a canonical YXXPhi motif with the clathrin adaptors AP-1A and AP-1B. *Proc Natl Acad Sci USA* **109:** 3820–3825.

Chan, Y.K., Huang, I.C., and Farzan, M. (2012) IFITM proteins restrict antibody-dependent enhancement of dengue virus infection. *PLoS ONE* **7:** e34508.

Diamond, M.S., and Farzan, M. (2013) The broad-spectrum antiviral functions of IFIT and IFITM proteins. *Nat Rev Immunol* **13:** 46–57.

Everitt, A.R., Clare, S., Pertel, T., John, S.P., Wash, R.S., Smith, S.E., *et al*. (2012) IFITM3 restricts the morbidity and mortality associated with influenza. *Nature* **484:** 519–523.

Feeley, E.M., Sims, J.S., John, S.P., Chin, C.R., Pertel, T., Chen, L.M., *et al*. (2011) IFITM3 inhibits influenza A virus infection by preventing cytosolic entry. *PLoS Pathog* **7:** e1002337.

Folsch, H., Pypaert, M., Schu, P., and Mellman, I. (2001) Distribution and function of AP-1 clathrin adaptor complexes in polarized epithelial cells. *J Cell Biol* **152:** 595–606.

Hickford, D.E., Frankenberg, S.R., Shaw, G., and Renfree, M.B. (2012) Evolution of vertebrate interferon inducible transmembrane proteins. *BMC Genomics* **13:** 155.

Hirst, J., Barlow, L.D., Francisco, G.C., Sahlender, D.A., Seaman, M.N., Dacks, J.B., and Robinson, M.S. (2011) The fifth adaptor protein complex. *PLoS Biol* **9:** e1001170.

Huang, I.C., Bailey, C.C., Weyer, J.L., Radoshitzky, S.R., Becker, M.M., Chiang, J.J., *et al*. (2011) Distinct patterns of IFITM-mediated restriction of filoviruses, SARS coronavirus, and influenza A virus. *PLoS Pathog* **7:** e1001258.

Jia, R., Pan, Q., Ding, S., Rong, L., Liu, S.L., Geng, Y., *et al*. (2012) The N-terminal region of IFITM3 modulates its antiviral activity by regulating IFITM3 cellular localization. *J Virol* **86:** 13697–13707.

Jiang, D., Weidner, J.M., Qing, M., Pan, X.B., Guo, H., Xu, C., *et al*. (2010) Identification of five interferon-induced cellular proteins that inhibit west nile virus and dengue virus infections. *J Virol* **84:** 8332–8341.

John, S.P., Chin, C.R., Perreira, J., Feeley, E.M., Aker, A., Savidis, G., *et al*. (2013) The CD225 domain of IFITM3 is required for both IFITM protein association and inhibition of influenza A virus and dengue virus replication. *J Virol* **87:** 7837–7852.

Lewin, A.R., Reid, L.E., McMahon, M., Stark, G.R., and Kerr, I.M. (1991) Molecular analysis of a human interferon-inducible gene family. *Eur J Biochem* **199:** 417–423.

Li, K., Markosyan, R.M., Zheng, Y.M., Golfetto, O., Bungart, B., Li, M., *et al*. (2013) IFITM proteins restrict viral membrane hemifusion. *PLoS Pathog* **9:** e1003124.

Lu, J., Pan, Q., Rong, L., He, W., Liu, S.L., and Liang, C. (2011) The IFITM proteins inhibit HIV-1 infection. *J Virol* **85:** 2126–2137.

Macia, E., Ehrlich, M., Massol, R., Boucrot, E., Brunner, C., and Kirchhausen, T. (2006) Dynasore, a cell-permeable inhibitor of dynamin. *Dev Cell* **10:** 839–850.

Mercer, J., Schelhaas, M., and Helenius, A. (2010) Virus entry by endocytosis. *Annu Rev Biochem* **79:** 803–833.

Mills, T.C., Rautanen, A., Elliott, K.S., Parks, T., Naranbhai, V., Ieven, M.M., *et al*. (2013) IFITM3 and susceptibility to respiratory viral infections in the community. *J Infect Dis*. doi:10.1093 [Epub ahead of print].

Moffatt, P., Gaumond, M.H., Salois, P., Sellin, K., Bessette, M.C., Godin, E., *et al*. (2008) Bril: a novel bone-specific modulator of mineralization. *J Bone Miner Res* **23:** 1497–1508.

Perreira, J.M., Chin, C.R., Feeley, E.M., and Brass, A.L. (2013) IFITMs restrict the replication of multiple pathogenic viruses. *J Mol Biol* **425:** 4937–4955.

Rous, B.A., Reaves, B.J., Ihrke, G., Briggs, J.A., Gray, S.R., Stephens, D.J., *et al*. (2002) Role of adaptor complex AP-3 in targeting wild-type and mutated CD63 to lysosomes. *Mol Biol Cell* **13:** 1071–1082.

Schoggins, J.W., and Randall, G. (2013) Lipids in innate antiviral defense. *Cell Host Microbe* **14:** 379–385.

Schoggins, J.W., Wilson, S.J., Panis, M., Murphy, M.Y., Jones, C.T., Bieniasz, P., and Rice, C.M. (2011) A diverse range of gene products are effectors of the type I interferon antiviral response. *Nature* **472:** 481–485.

Seachrist, J.L., Laporte, S.A., Dale, L.B., Babwah, A.V., Caron, M.G., Anborgh, P.H., and Ferguson, S.S. (2002) Rab5 association with the angiotensin II type 1A receptor promotes Rab5 GTP binding and vesicular fusion. *J Biol Chem* **277:** 679–685.

Siegrist, F., Ebeling, M., and Certa, U. (2011) The small interferon-induced transmembrane genes and proteins. *J Interferon Cytokine Res* **31:** 183–197.

Vazquez-Calvo, A., Saiz, J.C., McCullough, K.C., Sobrino, F., and Martin-Acebes, M.A. (2012) Acid-dependent viral entry. *Virus Res* **167:** 125–137.

Vercauteren, D., Vandenbroucke, R.E., Jones, A.T., Rejman, J., Demeester, J., De Smedt, S.C., *et al*. (2010) The use of inhibitors to study endocytic pathways of gene carriers: optimization and pitfalls. *Mol Ther* **18:** 561–569.

Wakim, L.M., Gupta, N., Mintern, J.D., and Villadangos, J.A. (2013) Enhanced survival of lung tissue-resident memory CD8(+) T cells during infection with influenza virus due to selective expression of IFITM3. *Nat Immunol* **14:** 238–245.

Weidner, J.M., Jiang, D., Pan, X.B., Chang, J., Block, T.M., and Guo, J.T. (2010) Interferon-induced cell membrane proteins, IFITM3 and tetherin, inhibit vesicular stomatitis virus infection via distinct mechanisms. *J Virol* **84:** 12646–12657.

Yount, J.S., Moltedo, B., Yang, Y.Y., Charron, G., Moran, T.M., Lopez, C.B., and Hang, H.C. (2010) Palmitoylome profiling reveals S-palmitoylation-dependent antiviral activity of IFITM3. *Nat Chem Biol* **6:** 610–614.

Yount, J.S., Karssemeijer, R.A., and Hang, H.C. (2012) S-palmitoylation and ubiquitination differentially regulate interferon-induced transmembrane protein 3 (IFITM3)-

mediated resistance to influenza virus. *J Biol Chem* **287:** 19631–19641.

Zhang, Y.H., Zhao, Y., Li, N., Peng, Y.C., Giannoulatou, E., Jin, R.H., *et al.* (2013) Interferon-induced transmembrane protein-3 genetic variant rs12252-C is associated with severe influenza in Chinese individuals. *Nat Commun* **4:** 1418.

Supporting information

Additional Supporting Information may be found in the online version of this article at the publisher's web-site:

Fig. S1. The N-Flag IFITM3 is not stained by anti-Flag antibody at the cell surface. N-Flag IFITM3 and YLAA were expressed in HEK293 cells. Detailed legend refers to Fig. 1C.

Fig. S2. Detecting the endocytosis of C-Myc IFITM3 in the antibody uptake assay. Myc tag was added to the N- or C-terminus of IFITM3 and the YLAA mutant.

A. Cell surface staining of C-Myc IFITM3 and the YLAA mutant with anti-Myc antibody. The wild-type IFITM3, but not YLAA, is able to undergo endocytosis.

B. The anti-Myc antibody cannot detect N-Myc IFITM3 at the cell surface.

Fig. S3. Results of flow cytometry analysis of IAV-infected HEK293 cells that express IFITM3 and its mutants YLAA, Y20A or L23A. These data are summarized in Fig. 5B. The amounts of IAV (in μl) used in each infection are indicated. The cells were harvested 8 h post infection and immunostained with anti-NP antibody.

Table S1. List of primers used in mutagenesis and cloning.